Roles of saltation, sandblasting, and wind speed variability on mineral dust aerosol size distribution during the Puerto Rican Dust Experiment (PRIDE)

Alf Grini
Department of Geosciences, University of Oslo, Oslo, Norway

Charles S. Zender
Department of Earth System Science, University of California, Irvine, California, USA

Received 9 October 2003; revised 15 December 2003; accepted 7 January 2004; published 2 April 2004.

[1] Recent field observations demonstrate that a significant discrepancy exists between models and measurements of large dust aerosol particles at remote sites. We assess the fraction of this bias explained by assumptions involving four different dust production processes. These include dust source size distribution (constant or dynamically changing according to saltation and sandblasting theory), wind speed distributions (using mean wind or a probability density function (PDF)), parent soil aggregate size distribution, and the discretization (number of bins) in the dust size distribution. The Dust Entrainment and Deposition global model is used to simulate the measurements from the Puerto Rican Dust Experiment (PRIDE) (2000). Using wind speed PDFs from observed National Centers for Environmental Prediction winds results in small changes in downwind size distribution for the production which neglects sandblasting, but it results in significant changes when production includes sandblasting. Saltation-sandblasting generally produces more large dust particles than schemes which neglect sandblasting. Parent soil aggregate size distribution is an important factor when calculating size-distributed dust emissions. Changing from a soil with large grains to a soil with smaller grains increases by 50% the fraction of large aerosols ($D > 5$ μm) modeled at Puerto Rico. Assuming that the coarse medium sand typical of West Africa dominates all source regions produces the best agreement with PRIDE observations. *INDEX TERMS:* 0305 Atmospheric Composition and Structure: Aerosols and particles (0345, 4801); 0340 Atmospheric Composition and Structure: Middle atmosphere—composition and chemistry; 0365 Atmospheric Composition and Structure: Troposphere—composition and chemistry; *KEYWORDS:* saltation, sandblasting, dust, aerosol, soil erosion, modeling

Citation: Grini, A., and C. S. Zender (2004), Roles of saltation, sandblasting, and wind speed variability on mineral dust aerosol size distribution during the Puerto Rican Dust Experiment (PRIDE), *J. Geophys. Res.*, *109*, D07202, doi:10.1029/2003JD004233.

1. Introduction

[2] Accurate representation of generation and long-range atmospheric transport of large particles is important for many aerosol species, including mineral dust, soot, sea salt, and ice crystals. Large particles (e.g., $D > 5$ μm, where D is the diameter of particle) usually account for a significant fraction of the mass distribution of most aerosols [e.g., *Zender and Kiehl*, 1994; *Seinfeld and Pandis*, 1997]. If dust mass concentration and deposition measurements are sensitive to relatively small numbers of relatively large particles [*Arimoto*, 2001], then so too are biogeochemical cycles in regions, such as the Southern Ocean [*Moore et al.*, 2002], influenced by dust-borne nutrients such as iron [*Martin*, 1990]. Global models of mineral dust distribution reproduce many observed features of the mass concentration and optical depth [e.g., *Tegen and Fung*, 1994; *Woodward*, 2001; *Ginoux et al.*, 2001; *Zender et al.*, 2003a]. However, there are not many detailed studies of the dust size distribution. Recent studies underpredict the observed size distributions of large dust particles after long-range transport [*Colarco et al.*, 2003; *Reid et al.*, 2003; *Ginoux*, 2003].

[3] Dust aerosols are produced by two related processes called saltation and sandblasting. Saltation is the net horizontal motion of large particles moving in a turbulent near-surface layer. Sandblasting is the release of dust and larger particles caused by saltators as they impact the surface. During impact, saltators may disintegrate or eject fine dust which is otherwise tightly bound to the soil or to the saltating soil aggregates themselves. These two processes are documented and discussed in several works [e.g., *Gomes et al.*, 1990; *Shao and Raupach*, 1993; *Alfaro et al.*, 1998; *Shao and Lu*, 2000; *Alfaro and Gomes*, 2001]. Models can best predict the size distribution of the dust (vertical) flux by first predicting the size distribution of the saltation (horizontal) flux.

0148-0227/04/2003JD004233$09.00

[4] Large-scale transport models have trouble reproducing the transport of large dust particles measured in remote stations [*Colarco et al.*, 2003; *Reid et al.*, 2003]. Asian mineral dust particles $D > 20$ μm have been measured at Mauna Loa [*Perry and Cahill*, 1999]. During the Intercontinental Transport and Chemical Transformation Field Mission, spring 2002, the mass median diameter (MMD) of springtime east Asian dust reaching the west coast of North America was >5 μm (K. Perry, personal communication, 2003). *Reid et al.* [2003] compared several measurement techniques during the Puerto Rican Dust Experiment (PRIDE) campaign (2000). Large dust particles were measured throughout the campaign. After evaluating optical and mass-based techniques they found that their best estimate of dust MMD in Barbados is 3.5 μm. Using only optical measurement techniques increases this estimate. Using only aerodynamic measurement techniques decreases it slightly.

[5] Recent research has partially addressed the problem of why models do not predict enough large particles at remote sites. *Colarco et al.* [2003] evaluated modeled size distributions and compared them to measured Aerosol Robotic Network (AERONET) size distributions. They point to several factors which impact the dust size distribution at Barbados: (1) the size distribution of the emissions (in the cases where more large particles are emitted, more large particles are also observed at Barbados) and (2) particle fall speed (aerosols which are not spheres fall slower than spheres). Using fall speed of disks rather than spheres, large aerosol concentration at Barbados increases. They found that only the source size distribution of *Ginoux et al.* [2001] combined with disk fall speed gave reasonable size distributions. However, the production scheme of *Ginoux et al.* [2001] does not produce dust by saltation and sandblasting. *Ginoux* [2003] showed that a moment-conserving advection scheme [*Prather*, 1986] reduces losses due to gravitational settling. This explains some of the too large loss of large particles seen in models.

[6] Three approaches for modeling the size-distributed dust production appear in the literature:

[7] 1. Empirical equations relate the size-distributed vertical dust flux to the wind speed [*Tegen and Fung*, 1994; *Ginoux et al.*, 2001; *Woodward*, 2001]. This approach includes a variety of ad hoc prescriptions and predictions of size distributions but does not account for the saltation-sandblasting process. *Ginoux et al.* [2001] use a threshold wind friction speed u_{*t} that increases with dust aerosol diameter. *Woodward* [2001] calculates saltation fluxes of all soil sizes and converts them to dust fluxes of the same size, assuming dust fluxes of a certain size are proportional to soil fluxes.

[8] 2. Saltation flux is explicitly calculated and used to prescribe a vertical dust flux through empirical relationships. This "halfway" approach explicitly represents saltation but not sandblasting. Studies which employ this approach often distribute the vertical dust flux into three lognormal modes with different shapes and mass fractions [*Marticorena et al.*, 1997; *Schulz et al.*, 1998; *Zender et al.*, 2003a].

[9] 3. Saltation and sandblasting are both explicitly represented and interact in a physical way to produce the emitted dust size distribution [*Shao et al.*, 1996; *Shao and Leslie*, 1997; *Gong et al.*, 2003]. To our knowledge, only two distinct methods which take this approach have been proposed [*Shao and Raupach*, 1993; *Shao*, 2001; *Alfaro and Gomes*, 2001].

Table 1. Lognormal Size Distributions of Dust Produced by Saltation and Sandblasting[a]

	Lognormal Mode		
	1	2	3
	D'Almeida [1987]		
MMD, μm	0.83	4.82	19.36
Standard deviation	2.10	1.90	1.60
Mass fraction	0.036	0.957	0.007
	Claquin [1999]		
MMD, μm	0.011	2.54	42.10
Standard deviation	1.89	2.0	2.13
Mass fraction	2.6×10^{-6}	0.78	0.22
	Alfaro and Gomes [2001]		
MMD, μm	1.5	6.7	14.2
Standard deviation	1.7	1.6	1.5
Mass fraction	varies	varies	varies

[a]MMD, mass median diameter.

[10] Table 1 shows size distributions representative of the latter two approaches. The mode with MMD ~2.5 μm is widely cited as important in dust emissions [*Shettle*, 1984; *Schulz et al.*, 1998; *Guelle et al.*, 2000; *Myhre et al.*, 2003]. However, there is no physical reason for a constant mode of this size. Saltation-sandblasting theory predicts time-varying dust size distributions dependent on soil properties and meteorology.

[11] Previous studies show that approaches 1 and 2 adequately simulate observed dust distributions on regional [*Marticorena et al.*, 1997] and global [*Ginoux et al.*, 2001; *Zender et al.*, 2003a] scales. Regional simulations using approach 3 [*Shao and Leslie*, 1997; *Gong et al.*, 2003] show that saltation-sandblasting explains continental-scale dust emissions well. Until now, global simulations using saltation-sandblasting microphysics have not been conducted. Our first objective is to show whether saltation-sandblasting production explains the observed size distribution of long-range dust better than other approaches and mechanisms. We find that it does. Moreover, saltation-sandblasting produces dust size distributions very sensitive to surface winds. Thus our second objective is to show whether saltation-sandblasting forced by realistic wind speed distributions explains the observed size distribution of long-range dust better than forcing with mean winds.

[12] The paper is organized as follows. Section 2 describes the dust production simulations and the measurements used to evaluate them. Section 3 presents the PRIDE simulations. Section 4 summarizes the conclusions of the study.

2. Theory and Methods

2.1. Dust Productions

[13] To our knowledge this study is the first intercontinental simulation of dust production and transport using saltation-sandblasting theory. Our PRIDE simulations employ a series of increasingly complex (and, we be-

lieve, more realistic) representations of dust production mechanisms:

[14] 1. Using saltation production, saltation is explicitly represented, though sandblasting is not. Size distribution of source emissions is prescribed from observations.

[15] 2. Using dynamical dust production, saltation and sandblasting are explicitly represented using the method of *Alfaro and Gomes* [2001]. Large-scale (grid cell mean) winds determine dust production.

[16] 3. Using wind speed distribution, a probability density function of wind speeds [*Justus et al.*, 1978] drives the dust production mechanism.

[17] The details of each production mechanism are presented below in sections 2.1.1–2.1.3.

2.1.1. Saltation-Only Production

[18] The control production method (CTL) is documented and evaluated by *Zender et al.* [2003a, 2003b]. The saltation mass flux depends on the wind friction speed excess over the threshold speed for entrainment of optimally sized (D = 75 μm) particles [*White*, 1979; *Iversen and White*, 1982]. A globally uniform sandblasting mass efficiency [*Alfaro et al.*, 1997; *Marticorena and Bergametti*, 1995] converts the predicted saltation into a vertical dust flux. The dust flux has a (globally uniform) prescribed size distribution [*D'Almeida*, 1987] when entrained from the surface (see Table 1). Thus the CTL mechanism accounts for saltation and neglects sandblasting. The size distribution changes during transport because of size-dependent wet and dry deposition.

2.1.2. Saltation-Sandblasting Production

[19] Saltation-sandblasting (SS) produces dynamic dust size distributions using the formulation of *Alfaro and Gomes* [2001]. The size-distributed saltation flux changes with wind friction speed [*Iversen and White*, 1982; *Grini et al.*, 2002]. The dust aerosol size released by sandblasting depends on saltator kinetic energy. Thus the dust size distribution depends on the parent soil aggregate size distribution and the wind friction speed. High kinetic energy saltators release small dust aerosols, and low kinetic energy saltators release large dust aerosols [*Shao and Raupach*, 1993]. The soil aggregate size distribution is thus an important factor [*Alfaro and Gomes*, 2001]. The kinetic energy is proportional to the mass of the saltator (and the square of the friction speed). Therefore coarse-textured soils produce more saltators with high kinetic energy than fine-textured soils. The computational efficiency problems with this method noted by *Grini et al.* [2002] were solved by storing all parameters needed in precomputed lookup tables. The dust size distribution at the source is then a simple function of wind friction speed and soil size distribution. It is important to distinguish between two types of size distributions often confounded in dust modeling: soil texture is the fraction of sand, silt, and clay-sized particles measured by soil scientists after disaggregating the soil (e.g., ultrasonically in water). This study uses soil aggregate size distribution, the dry size distribution including aggregates. It is most appropriately measured by dry-sieving the soil. We assume globally uniform lognormal distributions [*Chatenet et al.*, 1996] because better data are not available at the global scale.

[20] In the CTL formulation, dust emissions commence at the saltation threshold friction velocity, $u_{*t} \approx 0.20$ m s^{-1}, which is also a widely cited threshold for dust emissions [*Marticorena and Bergametti*, 1995; *Marticorena et al.*, 1997]. The SS formulation [*Alfaro and Gomes*, 2001], in contrast, produces dust only once u_* 0.3 m s^{-1} (the sandblasting threshold). This difference in saltation and sandblasting thresholds causes a difference in the frequency of emissions since the CTL mechanism emits more readily than the SS mechanism. Section 3.2 discusses how this difference affects our results.

[21] Emission efficiencies also differ between experiments. *Zender et al.* [2003a] use a fixed mass sandblasting efficiency of $\alpha = 10^{-4}$ m^{-1} which corresponds to a soil clay content of 20% [*Gillette*, 1979]. The *Alfaro and Gomes* [2001] mass sandblasting efficiencies are generally less, and they depend on the instantaneous saltation-sandblasting process.

2.1.3. Probability Density Function Wind Speeds

[22] The probability density function (PDF) production mechanism uses a wind speed PDF rather than the grid cell mean wind speed to initiate dust entrainment. Following *Gillette and Passi* [1988], we assume average variability winds and construct a Weibull distribution with the National Centers for Environmental Prediction (NCEP) estimated mean wind speed $\bar{U}$ [*Justus et al.*, 1978]. The free parameters in the PDF are a shape factor k and a scale factor c (m s^{-1}):

$$k_r = 0.94\sqrt{\bar{U}_r} \tag{1}$$

$$c_r = \bar{U}_r[\Gamma(1 + 1/k)]^{-1}, \tag{2}$$

where the subscript r denotes quantities at reference height (10 m) and Γ is the gamma function.

[23] *Justus et al.* [1978] provide the method to transfer the shape parameter from the reference height z_r (10 m) to the midpoint height z_{atm}:

$$k_{\mathrm{atm}} = k_r[1 - 0.088\ln(z_r/10)]/[1 - 0.088\ln(z_{\mathrm{atm}}/10)]; \tag{3}$$

c_{atm} comes from equation (2) with values for midpoint height instead of reference height.

[24] We discretize the central 90% of the wind PDF. The minimum wind speed represented is slower than 95% of the winds, and the maximum wind speed is faster than 95% of the winds. The cutoff wind speeds come from the cumulative form of the Weibull distribution

$$p_W(U < U_t) = 1 - \exp\left[-\left(\frac{U_t}{c}\right)^k\right], \tag{4}$$

where $p_W(U < U_t)$ is the probability of wind speed U being slower than the threshold U_t. We discretize U into five bins, calculate dust production for each bin, and weight these production terms by the Weibull PDF.

[25] Figure 1 shows the Weibull wind speed PDF $p_W(U)$. The standard deviation of $p_W(U)$ increases faster than $\bar{U}$. Thus neglect of the wind speed PDF is a worse approximation for faster winds when dust emission is most important.

2.2. Numerical Tools for Dust Emission and Transport

2.2.1. Dust Entrainment and Deposition Model

[26] We use the Dust Entrainment and Deposition model (DEAD) [*Zender et al.*, 2003a] to calculate dust production

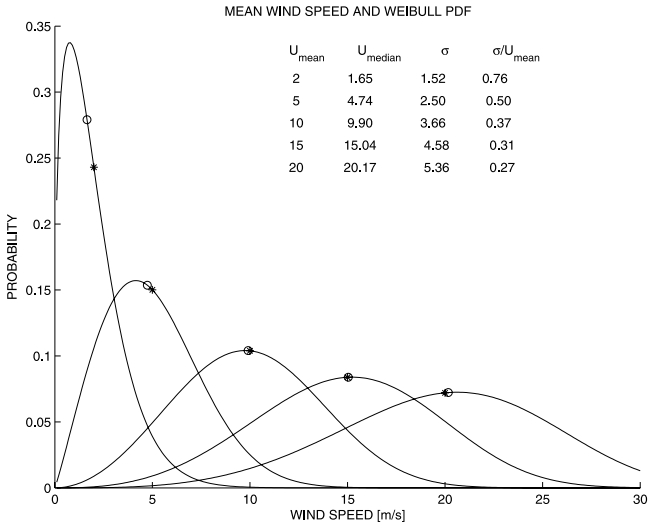

Figure 1. Weibull probability density function of wind speeds $p_W(U)$ for $\bar{U}$ = 2, 5, 10, 15, and 20 m s^{-1}. Mean and median winds are indicated on the curves with stars and circles, respectively.

and deposition. DEAD produces dust as a function of wind speed and stability in the boundary layer. A geomorphic erodibility factor accounts for spatial heterogeneity of dust sources [*Zender et al.*, 2003b]. Dust is transported using four size bins with boundaries at [0.1, 1.0, 2.5, 5.0, 10] μm. Simulations with more than four transport bins have boundaries logarithmically distributed between 0.1 and 10 μm. The distribution of mass in each bin is lognormal with mass median diameter of 2.5 μm and geometric standard deviation σ_g = 2.0. All properties specific to each bin (e.g., dry deposition velocity) are weighted according to this subgrid size distribution. In this study, DEAD has been expanded with a saltation-sandblasting module and a wind PDF module.

2.2.2. Transport Model

[27] The dust is transported in the Model of Atmospheric Transport and Chemistry chemical transport model [*Rasch et al.*, 1997] using time-interpolated 6-hourly meteorology from NCEP/National Center for Atmospheric Research reanalyses [*Kalnay*, 1996]. Wet and dry deposition processes remove more clay and silt-size particles, respectively. Nucleation and subcloud scavenging are treated separately with size-dependent scavenging coefficients which vary on the basis of the precipitation size distribution (stratiform or convective). Dry deposition uses a resistance method that incorporates gravitational, turbulent, and quasi-laminar terms [*Zender et al.*, 2003a].

2.2.3. Box Model Simulations

[28] Simulations with DEAD in box model mode demonstrate the effect of saltation and sandblasting on dust production. Table 2 shows the fraction of transported dust in each of the standard four size bins as a function of soil size distribution and wind speed. The soil types are described by *Chatenet et al.* [1996]. It can be seen that increasing the parent soil size increases the fraction of small dust produced (for a given wind speed). However, this is not a general conclusion, and it is dependent on the soil size distribution [*Grini et al.*, 2002].

2.3. Model-Constraining Measurements Performed During PRIDE

2.3.1. AERONET Sun Photometers

[29] AERONET Sun photometers estimate the column aerosol phase function and spectral optical depth from surface radiance measurements [*Dubovik and King*, 2000]. Column volume path V [m^3 m^{-2}] and aerosol optical depth (AOD) are retrieved from these measurements. The inversion procedure assumes the aerosol size distribution does not change with height. The retrieval error for the size distribution is 10–35% for intermediate size particles ($0.2 < D < 14$ μm) and increases to 80–100% outside this range [*Dubovik et al.*, 2000]. The absolute uncertainty in retrieved AOD is ±0.02. Thus the fractional error is large for low AOD and small for high AOD. The Sun photometers only measure during daylight. Plumes arriving at Puerto Rico during the night would not be measured unless they were still present the next noncloudy day.

2.3.2. Near-Surface Mass Concentration

[30] Observed dust mass concentrations are from University of Miami (UM) aerosol network observations. The instruments collect aerosol onto filters which are weighed before and after ashing. Dust concentration is estimated as the residual ash times 1.3, a factor that accounts for organic and volatile soil components. This technique agrees with independent estimates from Al measurements [*Arimoto et al.*, 1995; *Maring et al.*, 2003]. The upper size limit of UM measurements is about D = 30–40 μm.

[31] During PRIDE, concentration measurements were made between local noon (1600 UTC) and the following noon. Our model data are averages from 0000–2400 UTC. For UM data the time of midsample determines the measurement date. For most measured days, midsample occurred at ~0400 UTC. Our comparison may therefore

Table 2. Soil Type, Wind Speed, and Fraction of Transported Dust[a]

Soil Type[b]	Wind Speed,[c] m s^{-1}	Fraction 0.1–1.0 μm	1.0–2.5 μm	2.5–5.0 μm	5.0–10 μm
Dal87	all	0.03	0.17	0.40	0.38
ASS	6	0.0044	0.020	0.13	0.85
ASS	12	0.0083	0.032	0.14	0.82
ASS	18	0.0011	0.037	0.15	0.80
FS	6	0.0052	0.022	0.14	0.84
FS	12	0.012	0.042	0.15	0.79
FS	18	0.017	0.056	0.16	0.77
SS	6	0.011	0.038	0.15	0.80
SS	12	0.051	0.15	0.18	0.62
SS	18	0.093	0.26	0.19	0.46
CS	6	0.014	0.048	0.16	0.77
CS	12	0.080	0.23	0.19	0.50
CS	18	0.14	0.39	0.19	0.28

[a]Fraction of total $0.1 < D < 10$ μm dust produced in each bin.
[b]Sources: Dal87, "background mode," from *D'Almeida* [1987] and all other soil types from *Chatenet et al.* [1996]. ASS, aluminosilicated silt; FS, fine sand; SS, salts and clay; CS, coarse sand.
[c]Wind speed of 10 m (mean of Weibull PDF).

Table 3. Mobilization Processes in Each Simulation

Simulation	Production Mechanism	Number of Transport Bins	Wind[a]	Soil Size Distribution[b]
CTL	saltation only	4	mean	CMS
CTL10	saltation only	10	mean	CMS
CTLPDF	saltation only	4	PDF	CMS
SS	saltation-sandblasting	4	mean	CMS
SSPDF	saltation-sandblasting	4	PDF	CMS
SSPDFSFS	saltation-sandblasting	4	PDF	SFS

[a]Mean, time-interpolated NCEP wind; PDF, time-interpolated NCEP wind, which is mean of diagnosed Weibull PDF [*Justus et al.*, 1978].
[b]CMS, coarse medium sand; SFS, silty fine sand [*Marticorena et al.*, 1997].

be inconsistent occasionally, especially on days when dust arrived late in the evening.

2.3.3. Near-Surface Size Distribution

[32] The observed near-surface size distribution measurements are from the University of Utah (K. Perry, personal communication, 2002). These size distributions were retrieved using an eight-stage Davis Rotating Unit Monitoring (DRUM) impactor. DRUM and multiorifice uniform deposit impactors (MOUDI) had trouble measuring all large particles during PRIDE [*Reid et al.*, 2003]. The inlet aerodynamics of DRUM impactors have subsequently been changed to alleviate this problem (K. Perry, personal communication, 2003). However, DRUM aerodynamic measurements probably underestimate the mass fraction of particles with $D > 5$ μm during PRIDE. For these reasons we use DRUM measurements primarily for size distribution estimates. We present the DRUM total concentration measurements for informational purposes only and as an indication of sampling uncertainty. We convert the DRUM size-distributed Si concentration measurements to dust mass size distribution assuming the measured dust has a constant, size-independent Si mass fraction of 0.33 [*Seinfeld and Pandis*, 1997].

[33] The DRUM data do not measure the same thing as the UM filters. Our results show that three times measured Si (DRUM dust estimate) differs from 1.3 times measured ash (UM dust estimate). The UM concentrations are ~3 times higher, although the peak timings are very similar. This may be due to measuring different chemical species and/or to problems with the DRUM inlet size cutoff.

2.3.4. Evaluation Metrics

[34] There is a systematic bias between size distributions of dust retrieved from aerodynamic and from optical methods [*Reid et al.*, 2003]. Optical methods in general retrieve more aerosols of larger sizes. Thus simulation size distributions should be compared to both types of retrievals. We introduce two metrics, $\tilde{m}$ ($D > 5$) and $\tilde{V}$ ($D > 5$), for these comparisons:

$$\tilde{m}(D > 5\ \mu\text{m}) \equiv \frac{\int_{D=5}^{D=\infty} D^3 n_n(D) dD}{\int_{D=0}^{D=\infty} D^3 n_n(D) dD} = \frac{m(D > 5)}{m}, \qquad (5)$$

where $n_n(D)$ [m^{-3} m^{-1}] is the number distribution of dust, m [kg m^{-3}] is the total mass concentration of dust in the lowest model layer, and the metric $\tilde{m}$ ($D > 5$) is the fractional mass concentration of particles larger than five μm at measurement height (or in the lowest model layer). Aerodynamic methods, e.g., DRUM impactors, allow direct estimation of $\tilde{m}$ ($D > 5$).

[35] Similarly, surface remote-sensing methods allow direct estimation of column-integrated properties such as

$$\tilde{V}(D > 5\ \mu\text{m}) \equiv \frac{\int_{z=0}^{z=\infty} \int_{D=5}^{D=\infty} D^3 n_n(D,z) dD\ dz}{\int_{z=0}^{z=\infty} \int_{D=0}^{D=\infty} D^3 n_n(D,z) dD\ dz}, \qquad (6)$$

where z [m] is height and $\tilde{V}$ ($D > 5$) is the fractional volume path of dust particles larger than five μm in the atmospheric column. AERONET retrievals allow direct estimation of $\tilde{V}$ ($D > 5$) [*Dubovik and King*, 2000]. Together $\tilde{m}$ ($D > 5$) and $\tilde{V}$ ($D > 5$) provide convenient metrics to quantify the impact of dust production mechanism in each experiment on the large particles in the downwind size distribution.

2.4. Numerical Experiments

[36] Table 3 summarizes our numerical simulations. Model emissions were adjusted a posteriori to yield exact agreement between modeled and measured (by UM filters) PRIDE mean station concentrations at Roosevelt Roads. This makes the simulated size distributions easier to intercompare by eliminating the degree of freedom associated with absolute mass concentration.

2.4.1. Simulations With Saltation Dust Source

[37] Runs labeled CTL use the saltation size distribution for emissions. Two sensitivity tests were done with the CTL production formulation. The CTL10 sensitivity test used 10 transport bins instead of four. The size distribution of particles within each bin is unchanged; only the number of bins changes [*Zender et al.*, 2003a]. Differences between CTL10 and CTL results indicate the sensitivity of the transported size distribution to the number of transport bins. These differences arise from discretization of, e.g., dry deposition velocity and scavenging coefficients within a bin. The CTLPDF sensitivity test uses a prescribed subgridscale distribution of wind speeds to determine emissions rather than the grid cell mean wind speed. Dust emissions require wind speeds in excess of a threshold, and representing the wind speed PDF allows mobilization to occur in areas where the grid cell mean wind speed does not reach the threshold. Thus differences between CTLPDF and CTL results indicate the sensitivity of the size distribution to the wind speed distribution in source regions.

2.4.2. Simulations With Dynamical Dust Source

[38] In the SS and SSPDF simulations, all soils are assumed to be "coarse medium sand" (CMS) [*Chatenet et al.*, 1996; *Marticorena et al.*, 1997]. CMS is a blend of coarse sand (CS) (90% mass fraction, MMD = 690 μm, σ_g =

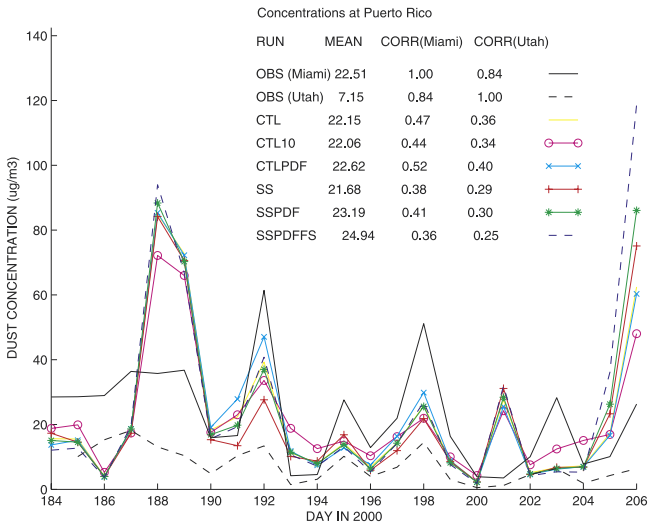

Figure 2. Near-surface dust mass concentration m [kg m^{-3}] at Roosevelt Roads, 2–24 July 2000. University of Miami measurements (solid black curve), University of Utah measurements (dashed black curve), CTL (yellow curve), CTL10 (magenta curve with circles), CTLPDF (cyan curve with crosses), SS (red curve with pluses), SSPDF (green curve with stars), and SSPDFSFS (dashed blue curve) are shown. Abbreviations are as follows: OBS, observed value; CORR or CORRCOEFF, correlation coefficient.

1.6) with fine sand (FS) (10% mass fraction, MMD = 210 μm, σ_g = 1.6). About 50% of the surface area of the western Sahara is CMS [*Marticorena et al.*, 1997]. The SS experiment uses the grid mean wind speed to predict emissions, while the SSPDF experiment uses Weibull PDF-distributed winds to predict emissions.

[39] The SSPDFSFS experiment assumes that the soil is "silty fine sand" (SFS) and that winds are Weibull distributed. SFS is a blend of fine sand (62.5% mass fraction) with aluminosilicated soils (ASS) (37.5% mass fraction, MMD = 125 μm, σ_g =1.8). SFS soils account for ~10% of the Western Sahara desert [*Marticorena et al.*, 1997]. The SSPDFSFS experiment shows the sensitivity of downwind dust distribution to soil size distribution in the source region. This sensitivity is largely determined by the efficiency of the sandblasting process.

[40] The mass fraction of each soil type is converted to a surface fraction using relations appropriate to the lognormal size distribution. We calculate a horizontal flux of each soil type for a given wind speed and weight this flux by the surface fraction covered by this soil type. The mass fraction of large soil aggregates is smaller than the surface fraction of large aggregates, since the larger aggregates have less surface per unit mass.

3. Results

3.1. Near-Surface Mass Concentration

[41] Figure 2 compares the measured mass concentration of dust at Roosevelt Roads in Puerto Rico to all simulations (see Table 3). The model predicts the correct number of peaks during PRIDE. The agreement is very good between model and measurements. Peaks on days 189, 192, 195, and 198 are well predicted by the model. The day 203 peak occurs 2 days early in the model. Figure 2 also shows total mass concentration based on Si measurements from the DRUM impactors. DRUM impactors measure less total concentration than the UM filters. DRUM and UM observations agree in timing but not in magnitude of dust events. This can be because of both different size cutoff and different chemical analysis (see sections 2.3.2 and 2.3.3).

3.2. Aerosol Optical Depth

[42] AERONET observations are available on nearly all days with significant cloud-free periods. We compute mean AOD and correlation coefficients to AERONET using only days when measured AOD is available. Figure 3 compares AERONET observations to the simulated AOD at Puerto Rico. The model underpredicts AOD during most dust events. The predicted timing is accurate for days 180 and 202 and too late on days 186 and 190. The model predicts two independent peaks on days 195 and 197 instead of the single peak observed on day 196.

[43] The observed optical depths are generally higher than the modeled ones. This is partially due to other natural aerosols (e.g., sea salt) or aerosols from industrial pollution or biomass burning. The 340/380 Ångstrøm exponent α for AOD measurements at Puerto Rico is ~0.5 for the periods of high optical depth during PRIDE. The low Ångstrøm exponent indicates that the aerosol is dust. The exponent α increases to 1.5–2.5 when optical depth is low (near 0.1). Thus ~0.1 of AOD may be explained by small aerosols including industrial pollution.

[44] Figure 4 compares the simulated AOD to AERONET observations at Cape Verde, ~700 km from the African continent. The SS and SSPDF production mechanisms yield unreasonably large optical depths at Cape Verde. Figure 4

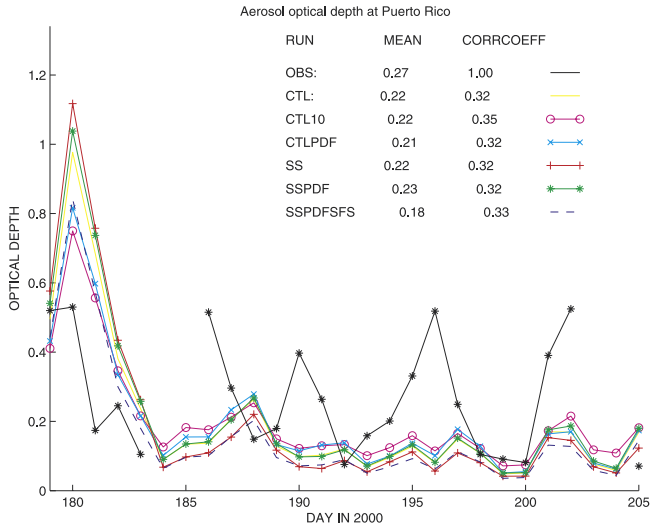

Figure 3. Aerosol optical depth at Roosevelt Roads, 27 June to 23 July 2000. AERONET measurements (black curve with stars), CTL (yellow curve), CTL10 (magenta curve with circles), CTLPDF (cyan curve with crosses), SS (red curve with pluses), SSPDF (green curve with stars), and SSPDFSFS (dashed blue curve) are shown.

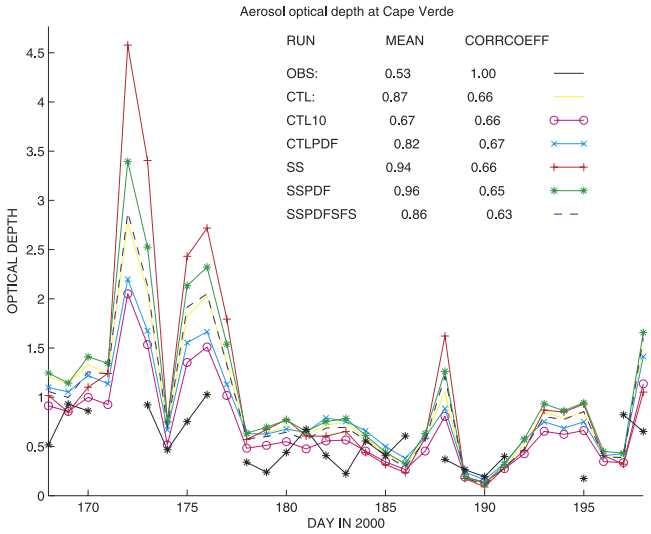

Figure 4. Aerosol optical depth at Cape Verde, 16 June to 16 July 2000. AERONET measurements (black curve with stars), CTL (yellow curve), CTL10 (magenta curve with circles), CTLPDF (cyan curve with crosses), SS (red curve with pluses), SSPDF (green curve with stars), and SSPDFSFS (dashed blue curve) are shown.

serves two purposes. First, it verifies that model and measured values reasonably agree for dust crossing Cape Verde. Much of the dust reaching Puerto Rico first crosses Cape Verde. The transit time from Sahara to Puerto Rico is ~5 days [*Mahowald et al.*, 2002; *Colarco et al.*, 2003]. To compare the same dust, the Cape Verde results are shown for an earlier period than results for Puerto Rico. A high correlation at Cape Verde 5 days before makes us confident that a high correlation at Puerto Rico is due to correct timing of dust production events.

[45] Second, Figure 4 verifies that emission frequency differences do not propagate far from the source region during the simulation period. As mentioned in section 2.1.2, the saltation-sandblasting formulations only emit dust when wind friction speeds exceed 0.3 m s^{-1}, whereas the saltation-only formulations produce dust when the wind friction speeds exceed 0.2 m s^{-1}. The simulated frequency of dust events crossing Cape Verde shows little sensitivity to the dust production formulation. Thus our simulated differences in dust production frequency either are small or do not influence dust concentrations close to the source. This is consistent with the findings of *Colarco et al.* [2003] that increasing wind speed threshold from the formulation of *Marticorena and Bergametti* [1995] (with u_{*t} = 0.2 m s^{-1}) to a fixed 10 m wind speed threshold ($U_{10,t}$ = 6.5 m s^{-1}) does not change the frequency but does change the magnitude of dust events.

[46] Figure 5 shows the covariation of observed mass concentration and AOD at Puerto Rico. Near-surface mass concentration peaks generally occur later than AOD maxima. We believe that the tropical easterly winds transport dust aloft more rapidly than near-surface dust. The lag causes the very low correlation coefficient ($r = -0.17$) even though both measurements clearly show the same dust events. The difference may also be due to UM sampling local noon to local noon, whereas AERONET measures during local daylight only.

3.3. Size Distributions From Sun Photometry

[47] Figure 6 shows the columnar volume distribution from AERONET Sun photometry and simulations. Size distributions are shown for days 187, 195, 197, and 202. Both model and observations show high optical depths on these days (Figure 3). The low bias in simulated silt-sized particles ($D > 2.5$ μm) approaches and often exceeds an order of magnitude for all production mechanisms. Locally produced sea salt and crustal aerosol may contribute to the observed silt-sized particles. The difference in size distribution is not only attributable to dust production. Errors in dry or wet deposition rates also influence the results. Since no production mechanism reproduces the flatness of the AERONET size distributions, our deposition rates of large aerosols may be too high.

[48] The fixed production formulations (CTL and CTL10) yield higher volume paths in the 1–5 μm size range. CTL10 yields more clay ($D < 2.5$ μm) particles than CTL because the wet scavenging coefficients for clay in CTL10 are not tuned as they are in the other simulations [*Zender et al.*, 2003a]. CTL10 averages the sedimentation velocity of each size over a narrower bin; thus large particles fall at speeds closer to reality. This explains the reduced volume in the largest sizes in CTL10. As we show in section 3.5, these differences due to bin discretization are small compared to changing from fixed to dynamical source schemes.

[49] Among dynamical schemes, SSPDF produces the most small aerosols, and SSPDFSFS produces the most large aerosols. Column volume paths of large sizes in the sandblasting simulations vary with the meteorological conditions during dust production. Figure 6 shows that SSPDFSFS consistently produces the most large particles. Small saltators dominate the SFS soil blend (see section 2.4.2) and

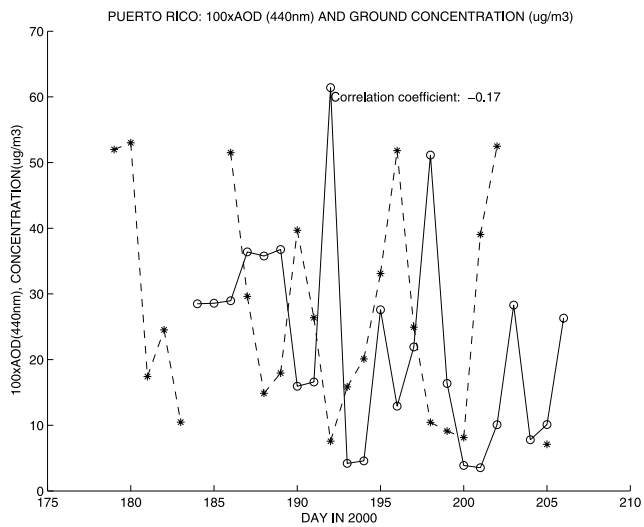

Figure 5. Covariation of observed optical depth and concentration at Puerto Rico. AOD (dashed curve with stars) is multiplied by 100. The mass concentrations (solid line with circles) are also shown.

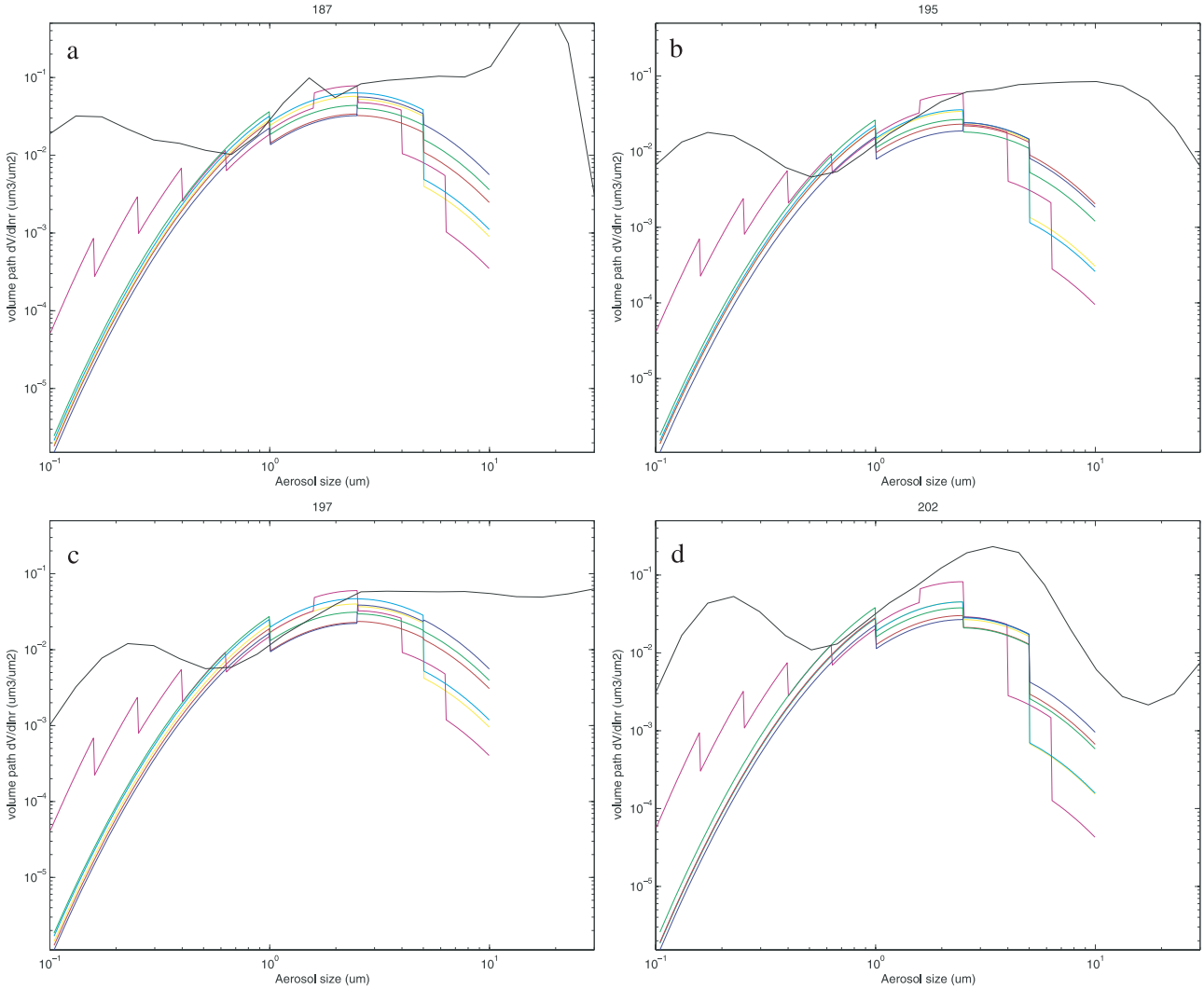

Figure 6. Columnar volume distributions $n_v(D)$ [m^3 m^{-2}] at Puerto Rico in 2000 for July (day of month)/(day of year) (a) 5/187, (b) 13/195, (c) 15/197, and (d) 20/202. Shown are measurements (black curve), CTL (yellow curve), CTL10 (magenta curve), CTLPDF (cyan curve), SS (red curve), SSPDF (green curve), and SSPDFSFS (blue curve).

preferentially sandblast large dust particles with low binding energies [*Alfaro and Gomes*, 2001]. Thus sandblasting theory demonstrates the sensitivity of the downwind size distribution to the soil size distribution in source regions, which is usually poorly constrained.

3.4. Near-Surface Size Distribution

[50] Next we contrast the observed (section 2.3.3) and modeled near-surface mass distributions. Figure 7 shows mass distributions for days 188, 189, 197, and 198. Both model and observations show relatively high concentration on these days (Figure 2). Saltation-sandblasting produces larger variations among events than saltation alone. The model predicts more dust than DRUM measurements because it is tuned to match UM dust concentration measurements which, in general, exceed the aggregated DRUM measurements.

[51] Note that SSPDFSFS consistently predicts the most large aerosols, while the differences between SS and SSPDF predictions depend on day and event. We also note an important aspect of using soil blends: Blending two soil size distributions does not result in a linear contribution from each soil proportional to their mass fractions. The effects of a small fraction of fine-textured soil may dominate the mass flux produced by a coarse-textured soil for two reasons:

[52] 1. Fine soils have larger influences than indicated by their mass fractions. We model the saltation flux from a soil as proportional to the surface covered by that soil. Even for small mass fractions of fine soil the surface fraction can be significant.

[53] 2. Fine soils sandblast more large aerosols, and coarse soils sandblast more small aerosols. Thus fine soils have much larger mass sandblasting efficiencies. Usually, the sandblasting performed by the fine soil fraction of a soil blend dominates the dust mass flux.

3.5. Fraction of Large Aerosols

[54] Figures 8 and 9 compare the mean observed and modeled $\tilde{m}$ ($D > 5$) and $\tilde{V}$ ($D > 5$) (equations (5) and (6)),

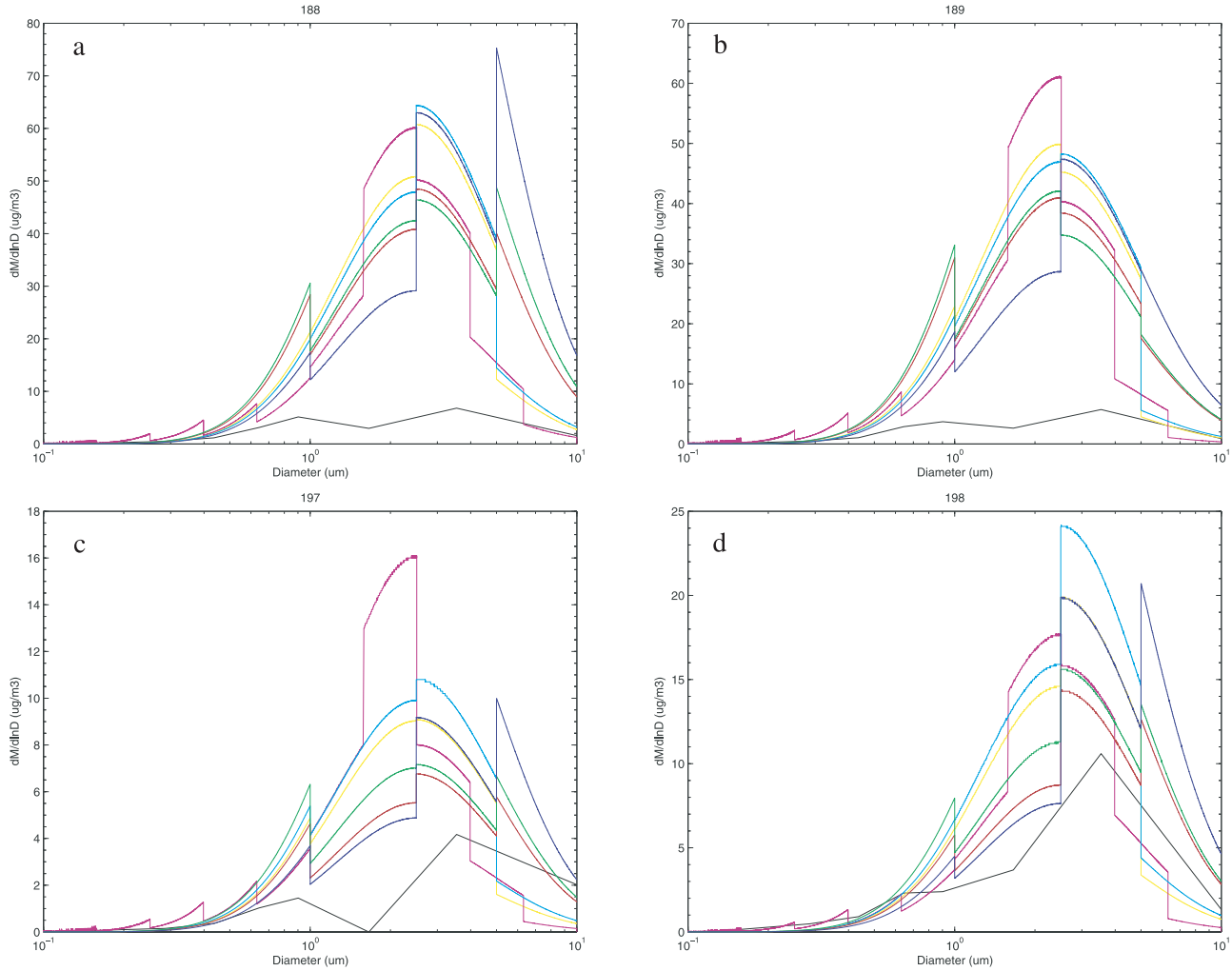

Figure 7. Near-surface mass distributions $n_m(D)$ [μg m^{-3}] at Puerto Rico in 2000 for July (day of month)/(day of year) (a) 6/188, (b) 7/189, (c) 15/197, and (d) 16/198. Shown are measurements (black curve), CTL (yellow curve), CTL10 (magenta curve), CTLPDF (cyan curve), SS (red curve), SSPDF (green curve), and SSPDFSFS (blue curve). Note difference in scales from Figures 7a to 7d.

respectively, for the PRIDE period. SS physics consistently produces more large aerosols than the saltation-only (CTL) mechanism. The SS source distribution contains modes with MMDs at 6.7 and 14.2 μm [*Alfaro and Gomes*, 2001]. These modes activate first as slower winds are required to exceed their threshold velocity. These modes are significantly larger than the 4.82 μm mass median dust diameter [*D'Almeida*, 1987] prescribed at the source in the CTL simulations. Prescribing a larger diameter at the source would produce more large aerosols at the source independent of wind speed. As mentioned in section 2.3.3, the DRUM size-resolved aerodynamic measurements may underestimate the mass fraction of particles with $D > 5$ μm. This would bring the $\tilde{m}$ ($D > 5$) (equation (5)) simulated by saltation-sandblasting processes into even better agreement with observations.

[55] Both the SS and the SSPDF experiments use the same soil size distribution, yet SSPDF transports fewer large aerosols. Sandblasting physics explain this outcome. In SSPDF a small but significant fraction of the winds are fairly fast (see Figure 1). Faster winds sandblast more small

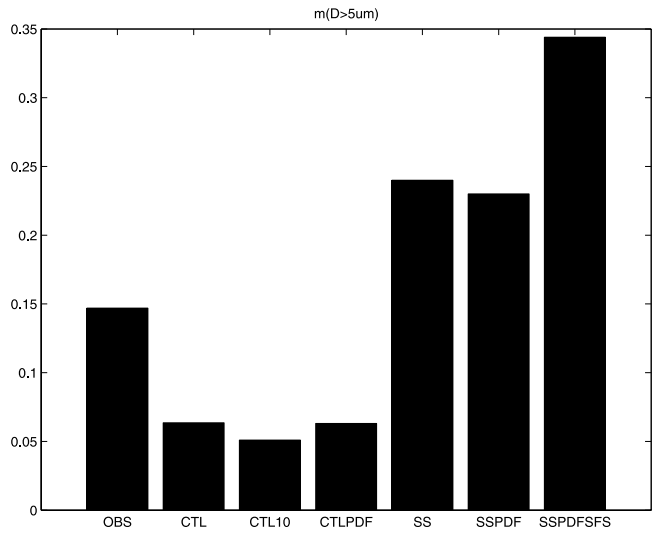

Figure 8. Observed and simulated $\tilde{m}$ ($D > 5$), the near-surface fractional mass concentration of particles larger than 5 μm.

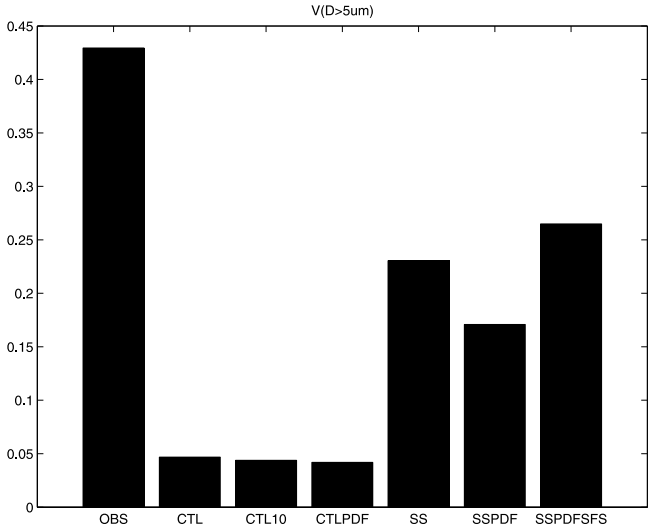

Figure 9. Observed and simulated $\tilde{V}$ ($D > 5$), the fractional volume path of dust particles larger than 5 μm.

aerosols than slower winds, provided that the saltators are large enough to exceed the binding energy of the finest dust. Sufficiently large saltators are required to sandblast fine dust. Increasing mean winds produces more small particles for the soil size distributions that we employ (Table 2), but this is not a general rule.

[56] The difference between SSPDF and SSPDFSFS is striking in Figures 8 and 9. Accurate predictions of sandblasting, and thus dust emissions and downwind size distributions, require detailed source soil size distribution data. These data must include the soil size distribution of all potential saltators; roughly $40 < D < 700$ μm [*Iversen and White*, 1982]. Remote sensing is one promising avenue for producing these data (G. S. Okin and T. H. Painter, unpublished data, 2003).

[57] Our subgridscale wind distribution, the Weibull distribution, is based on empirical parameterizations [*Justus et al.*, 1978] previously used in other wind erosion models [*Gillette and Passi*, 1988; *Shao et al.*, 1996]. In this formulation, wind speed standard deviation (and thus variability or gustiness) increases with the mean wind speed. Figure 1 shows that the standard deviation increases with the wind speed. However, the standard deviation decreases relative to the mean wind (from 76% for 2 m s^{-1} to 27% for 20 m s^{-1}). In reality, wind speed variability is also linked to boundary layer turbulence and to both dry and wet convection. Since these processes are simulated in three-dimensional meteorological models, they could be linked into the variability of the wind PDF (equation (2)).

[58] In 2002 the MMD of springtime east Asian dust did not change much between measurements at Gosan, Sea of Japan, and Crater Lake, Oregon, where it exceeded 5 μm after crossing the Pacific (K. Perry, personal communication, 2003). The transatlantic crossing time of African dust is ~5 days [*Mahowald et al.*, 2002; *Colarco et al.*, 2003], similar to the transpacific crossing time of Asian dust which is embedded in a stronger westerly flow. Table 4 shows the simulated change in monthly size distribution from the Saharan source region to Puerto Rico in the SSPDF simulation.

[59] The simulated fraction of aerosols larger than 5 μm decreases from 0.75 in emission to 0.53 in near-Sahara concentration to 0.14 in near-Puerto Rico concentration. Thus silty dust appears to settle or wash out much more rapidly in our model than in observations.

4. Conclusions

[60] Three different source formulations for dust production were used in a chemical transport model to simulate emissions and long-range transport of mineral dust during the PRIDE campaign. The model results were compared to measurements of aerosol size distribution, mass concentration, and optical depth from optical, aerodynamic, and filter instruments. Physically based sensitivity studies addressed the mechanisms which could explain why mineral dust emission and all known transport models underpredict long-range transport of the large particles [*Colarco et al.*, 2003; *Ginoux*, 2003] seen in observations [*Perry and Cahill*, 1999; *Reid et al.*, 2003].

[61] Previous model attempts to reproduce the large particle size distribution measured downwind of dust sources focused on aspherical particle shape effects and on improving advection schemes [*Colarco et al.*, 2003; *Ginoux*, 2003]. These studies left a significant fraction of the large particles unexplained. We showed that a production mechanism which accounts for saltation but neglects sandblasting underpredicts the fraction of particles larger than 5 μm observed after long-range transport. A production mechanism which accounts for saltation and sandblasting produces greater fractions of large particles in closer agreement with observations. Contingent on the sandblasting process and saltator population, realistic wind speed variability tends to reduce the emitted and transported fraction of large particles. Saltation-sandblasting, in conjunction with wind speed variability, significantly reduces, and in some cases eliminates, model biases in production and long-range transport of large dust particles.

[62] The observed fraction of long-range transported large aerosol ($D > 5$ μm) is the net result of a complex interaction of nonlinear processes where saltation-sandblasting and wind variability interact. Whether each process increases or decreases the mobilization of large particles depends on the values of the other and on the boundary conditions

Table 4. Change in Size Distribution During Transatlantic Transport

Region[a]	Day of Year	Property	Fraction			
			0.1–1.0 μm	1.0–2.5 μm	2.5–5.0 μm	5.0–10 μm
Sahara	170–200	production flux	0.021	0.069	0.16	0.75
Sahara	170–200	dust concentration	0.057	0.17	0.24	0.53
Puerto Rico	175–205	dust concentration	0.20	0.40	0.25	0.14

[a]Sahara, −20° < longitude < 35°E, 10° < latitude < 35°N; Puerto Rico, −90° < longitude < −60°E, 15° < latitude < 25°N.

(parent soil size distribution). Thus saltation-sandblasting and wind variability ought to be considered together. We conclude that a significant fraction of the remaining discrepancy is explained by interactions of saltation-sandblasting, wind variability, and soil size distribution in source regions.

[63] The downwind size distribution is very sensitive to the soil size distribution in source regions, which is usually poorly constrained. Assuming that most source soil is the coarse medium sand typical of West Africa produces the best agreement with observations during PRIDE. This study points out the need for an improved global soil size distribution data set that goes beyond the sand, silt, and clay texture classification traditionally used by soil scientists. The data set must include as much information as possible on the soil size distribution of all potential saltators; roughly $40 < D < 700$ μm [*Iversen and White*, 1982]. To reproduce observations, global models must predict the correct emitted size distribution and size-dependent deposition processes during transport. Since reliable soil size distribution and wind variability data are unavailable globally, it is difficult to assess whether global dust transport models err more in production or in transport. The ideal experiment to isolate these processes would be Lagrangian monitoring of dust in a transoceanic plume.

[64] **Acknowledgments.** A.G. acknowledges support from the Norwegian research council grant 139810/720 (CHEMCLIM). C.S.Z. gratefully acknowledges support from NASA grants NAG5-10147 (IDS) and NAG5-10546 (NIP). We thank Kevin Perry (University of Utah) and Dennis Savoie and Hal Maring (University of Miami) for sharing their data. We thank Jeff Reid and all the organizers and contributors to PRIDE for coordinating this useful experiment. Comments from two anonymous reviewers helped improve this paper.

References

Alfaro, S. C., and L. Gomes (2001), Modeling mineral aerosol production by wind erosion: Emission intensities and aerosol size distributions in source areas, *J. Geophys. Res.*, *106*, 18,075–18,084.

Alfaro, S. C., A. Gaudichet, L. Gomes, and M. Maillé (1997), Modeling the size distribution of a soil aerosol produced by sandblasting, *J. Geophys. Res.*, *102*, 11,239–11,249.

Alfaro, S. C., A. Gaudichet, L. Gomes, and M. Maillé (1998), Mineral aerosol production by wind erosion: Aerosol particle sizes and binding energies, *Geophys. Res. Lett.*, *25*, 991–994.

Arimoto, R. (2001), Eolian dust and climate: Relationships to sources, tropospheric chemistry, transport and deposition, *Earth Sci. Rev.*, *54*, 29–42.

Arimoto, R., R. A. Duce, B. J. Ray, W. G. Ellis Jr., J. D. Cullen, and J. T. Merrill (1995), Trace elements in the atmosphere over the North Atlantic, *J. Geophys. Res.*, *100*, 1199–1213.

Chatenet, B., M. Marticorena, L. Gomes, and G. Bergametti (1996), Assessing the microped size distributions of desert soils erodible by wind, *Sedimentology*, *43*, 901–911.

Claquin, T. (1999), Modelisation de la mineralogie et du forcage radiatif des poussieres desertiques, Ph.D. thesis, Univ. of Hamburg, Hamburg, Germany.

Colarco, P. R., O. B. Toon, and B. N. Holben (2003), Saharan dust transport to the Caribbean during PRIDE: 1. Influence of dust sources and removal mechanisms on the timing and magnitude of downwind aerosol optical depth events from simulations of in situ and remote sensing observations, *J. Geophys. Res.*, *108*(D19), 8589, doi:10.1029/2002JD002658.

D'Almeida, G. A. (1987), On the variablility of desert aerosol radiative characteristics, *J. Geophys. Res.*, *92*, 3017–3026.

Dubovik, O., and M. King (2000), A flexible inversion algorithm for retrievel of aerosol optical properties from Sun and sky radiance measurements, *J. Geophys. Res.*, *105*, 20,673–20,696.

Dubovik, O., A. Smirnov, B. Holben, M. King, Y. Kaufman, T. Eck, and I. Slutsker (2000), Accuracy assessments of aerosol optical properties retrieved from Aerosol Robotic Network (AERONET) Sun and sky radiance measurements, *J. Geophys. Res*, *105*, 9791–9806.

Gillette, D. (1979), Environmental factors affecting dust emission by wind erosion, in *Saharan Dust*, edited by C. Morales, pp. 71–94, John Wiley, Hoboken, N. J.

Gillette, D. A., and R. Passi (1988), Modeling dust emission caused by wind erosion, *J. Geophys. Res.*, *93*, 14,233–14,242.

Ginoux, P. (2003), Effects of nonsphericity on mineral dust modeling, *J. Geophys. Res.*, *108*(D2), 4052, doi:10.1029/2002JD002516.

Ginoux, P., M. Chin, I. Tegen, J. Prospero, B. Holben, O. Dubovik, and S.-J. Lin (2001), Sources and distributions of dust aerosols simulated with the GOCART model, *J. Geophys. Res.*, *106*, 20,255–20,273.

Gomes, L., G. Bergametti, G. Coudé-Gaussen, and P. Rognon (1990), Submicron desert dusts: A sandblasting process, *J. Geophys. Res.*, *95*, 13,927–13,935.

Gong, S. L., X. Y. Zhang, T. L. Zhao, I. G. McKendry, D. A. Jaffe, and N. M. Lu (2003), Characterization of soil dust aerosol in China and its transport and distribution during 2001 ACE-Asia: 2. Model simulation and validation, *J. Geophys. Res.*, *108*(D9), 4262, doi:10.1029/2002JD002633.

Grini, A., C. S. Zender, and P. R. Colarco (2002), Saltation sandblasting behavior during mineral dust aerosol production, *Geophys. Res. Lett.*, *29*(18), 1868, doi:10.1029/2002GL015248.

Guelle, W., Y. J. Balkanski, M. Schulz, B. Marticorena, G. Bergametti, C. Moulin, R. Arimoto, and K. D. Perry (2000), Modeling the atmospheric distribution of mineral aerosol: Comparison with ground measurements and satellite observations for yearly and synoptic timescales over the North Atlantic, *J. Geophys. Res.*, *105*, 1997–2012.

Iversen, J. D., and B. R. White (1982), Saltation threshold on Earth, Mars, and Venus, *Sedimentology*, *29*, 111–119.

Justus, C., W. Hargraves, A. Mikhail, and D. Graber (1978), Methods for estimating wind speed frequency distributions, *J. Appl. Meteorol.*, *17*, 350–353.

Kalnay, E. (1996), The NCEP/NCAR 40-year reanalysis project, *Bull. Am. Meteorol. Soc.*, *77*, 437–471.

Mahowald, N. M., C. S. Zender, C. Luo, D. Savoie, O. Torres, and J. del Corral (2002), Understanding the 30-year Barbados desert dust record, *J. Geophys. Res.*, *107*(D21), 4561, doi:10.1029/2002JD002097.

Maring, H., D. L. Savoie, M. A. Izaguirre, L. Custals, and J. S. Reid (2003), Mineral dust aerosol size distribution change during atmospheric transport, *J. Geophys. Res.*, *108*(D19), 8592, doi:10.1029/2002JD002536.

Marticorena, B., and G. Bergametti (1995), Modeling the atmospheric dust cycle: 1. Design of a soil-derived dust emission scheme, *J. Geophys. Res.*, *100*, 16,415–16,430.

Marticorena, B., G. Bergametti, B. Aumont, Y. Callot, C. N'Doumé, and M. Legrand (1997), Modeling the atmospheric dust cycle: 2. Simulation of Saharan dust sources, *J. Geophys. Res.*, *102*, 4387–4404.

Martin, J. H. (1990), Glacial-interglacial CO_2 change: The iron hypothesis, *Paleoceanography*, *5*, 1–13.

Moore, J. K., S. C. Doney, D. M. Glover, and I. Y. Fung (2002), Iron cycling and nutrient-limitation patterns in surface waters of the world ocean, *Deep Sea Res., Part II*, *49*, 463–507.

Myhre, G., A. Grini, J. M. Haywood, F. Stordal, B. Chatenet, D. Tanr, J. K. Sundet, and I. S. A. Isaksen (2003), Modeling the radiative impact of mineral dust during the Saharan Dust Experiment (SHADE) campaign, *J. Geophys. Res.*, *108*(D18), 8579, doi:10.1029/2002JD002566.

Perry, K. D., and T. A. Cahill (1999), Long-range transport of anthropogenic aerosols to the National Oceanic and Atmospheric Administration baseline station at Mauna Loa Observatory, Hawaii, *J. Geophys. Res.*, *104*, 18,521–18,533.

Prather, M. J. (1986), Numerical advection by conservation of second-order moments, *J. Geophys. Res.*, *91*, 6671–6681.

Rasch, P., N. Mahowald, and B. Eaton (1997), Representations of transport, convection, and the hydrologic cycle in chemical transport models: Implications for the modeling of short-lived and soluble species, *J. Geophys. Res.*, *102*, 28,127–28,138.

Reid, J. S., et al. (2003), Comparison of size and morphological measurements of coarse mode dust particles from Africa, *J. Geophys. Res.*, *108*(D19), 8593, doi:10.1029/2002JD002485.

Schulz, M., Y. Balkanski, W. Guelle, and F. Dulac (1998), Role of aerosol size distribution and source location in a three-dimensional simulation of a Saharan dust episode tested against satellite-derived optical thickness, *J. Geophys. Res.*, *103*, 10,579–10,592.

Seinfeld, J. H., and S. N. Pandis (1997), *Atmospheric Chemistry and Physics*, John Wiley, Hoboken, N. J.

Shao, Y. (2001), A model for mineral dust erosion, *J. Geophys. Res.*, *106*, 20,239–20,254.

Shao, Y., and L. M. Leslie (1997), Wind erosion prediction over the Australian continent, *J. Geophys. Res.*, *102*, 30,091–30,105.

Shao, Y., and I. Lu (2000), A simple expression for wind erosion threshold friction velocity, *J. Geophys. Res.*, *105*, 22,437–22,443.

Shao, Y., and M. Raupach (1993), Effect of saltation bombardment by wind, *J. Geophys. Res.*, *98*, 12,719–12,726.

Shao, Y., M. R. Raupach, and J. F. Leys (1996), A model for predicting aeolian sand drift and dust entrainment on scales from paddock to region, *Aust. J. Soil Res.*, *34*, 309–342.

Shettle, E. P. (1984), Optical and radiative properties of a desert aerosol model, in *Proceedings of the Symposium on Radiation in the Atmosphere*, edited by G. Fiocco, pp. 74–77, A. Deepak Publ., Hampton, Va.

Tegen, I., and I. Fung (1994), Modeling of mineral dust in the atmosphere: Sources, transport, and optical thickness, *J. Geophys. Res.*, *99*, 22,897–22,914.

White, B. R. (1979), Soil transport by winds on Mars, *J. Geophys. Res.*, *84*, 4643–4651.

Woodward, S. (2001), Modeling the atmospheric life cycle and radiative impact of mineral dust in the Hadley Centre climate model, *J. Geophys. Res.*, *106*, 18,155–18,166.

Zender, C. S., and J. T. Kiehl (1994), Radiative sensitivities of tropical anvils to small ice crystals, *J. Geophys. Res.*, *99*, 25,869–25,880.

Zender, C. S., H. Bian, and D. Newman (2003a), Mineral Dust Entrainment and Deposition (DEAD) model: Description and 1990s dust climatology, *J. Geophys. Res.*, *108*(D14), 4416, doi:10.1029/2002JD002775.

Zender, C. S., D. J. Newman, and O. Torres (2003b), Spatial heterogeneity in aeolian erodibility: Uniform, topographic, geomorphic, and hydrologic hypotheses, *J. Geophys. Res.*, *108*(D17), 4543, doi:10.1029/2002JD003039.

A. Grini, Department of Geosciences, University of Oslo, P.O. Box 1022 Blindern, N-0315 Oslo, Norway. (alf.grini@geo.uio.no)

C. S. Zender, Department of Earth System Science, University of California, Irvine, CA 92697-3100, USA. (zender@uci.edu)